# Conversion of aquaporin 6 from an anion channel to a water-selective channel by a single amino acid substitution

Kun Liu*, David Kozono*, Yasuhiro Kato†, Peter Agre*‡, Akihiro Hazama§, and Masato Yasui*¶∥

Departments of *Biological Chemistry, ‡Medicine, and ¶Pediatrics, The Johns Hopkins University School of Medicine, Baltimore, MD 21205; †Cornea Center, Tokyo Dental College, Ichikawa, Chiba 272-8513, Japan; and §Department of Physiology, Fukushima Medical College, Fukushima 960-1295, Japan

Aquaporin (AQP) 6 belongs to the aquaporin water channel family. Unlike other aquaporins, AQP6 functions not as a water channel but as an anion-selective channel. Single-channel analyses have shown AQP6 to flicker rapidly between closed and open status. The atomic structure of AQP1 and amino acid sequence alignments of the mammalian aquaporins reveal two well conserved glycine residues: Gly-57 in transmembrane helix (TM) 2 and Gly-173 in TM5 reside at the contact point where the two helices cross in human AQP1. Uniquely, all known mammalian orthologs of AQP6 have an asparagine residue (Asn-60) at the position corresponding to Gly-57. Here we show that a single residue substitution (N60G in rat AQP6) totally eliminates the anion permeability of AQP6 when expressed in *Xenopus* oocytes, but the N60G oocytes exhibit significantly higher osmotic water permeability under basal conditions. Replacement of the glycine at this site in AQP0, AQP1, and AQP2 blocked expression of the mutants at the oocyte plasma membrane. We propose that the asparagine residue at the contact point between TM2 and TM5 in AQP6 may function as a teeter board needed for rapid structural oscillations during anion permeation.

anion permeability | structure–function | water permeability

The aquaporins are a family of integral membrane proteins that function largely as water channels at the plasma membranes of cells (1). Ion permeability, including hydronium ions, is not a general feature of aquaporins (2–7). We recently demonstrated, however, that aquaporin (AQP) 6 functions not as a water channel but as an anion channel with the halide permeability sequence: $NO_3^- > I^- \gg Br^- > Cl^- \gg F^-$ (8, 9). When expressed in *Xenopus laevis* oocytes, AQP6 exhibited minimal water permeability. In mammalian cells expressing GFP-tagged AQP6, outward rectifying currents were induced after replacing NaCl with $NaNO_3$ in the bath solution. Moreover, we showed that AQP6 is a gated channel by single-channel patch recording with oocyte membranes expressing AQP6 (10). The unique functions of AQP6 may be due to its distinct structure, especially in the formation of its pore.

The atomic structure of AQP1 has been established by electron crystallography and x-ray crystallography (11, 12). AQP1 exists as a tetramer with each subunit containing its own pore. The hourglass-shaped pore is formed by two loops, each containing a highly conserved NPA motif and a short helix and by a right-handed bundle of six highly tilted α-helices. There are three sites where helices cross, between helices 1 and 3, 4 and 6, and 2 and 5. All three have highly conserved glycine residues at the contact sites, and this is thought to stabilize the monomer (13). The atomic structure and molecular dynamics simulations of AQP1 provide a uniquely selective mechanism for free permeation by water through the channel pore and a mechanism for proton blockage: (*i*) size restriction at the narrowest constriction of the pore; (*ii*) electrostatic repulsion by the well conserved arginine residue right after the second NPA motif; and (*iii*) water dipole reorientation at the midpoint of the pore,

## Table 1. Site-directed mutations

| Mutation | WT | | Mutant | |
|---|---|---|---|---|
| | Amino acid | Codon | Amino acid | Codon |
| AQP6 N60G | Asn-60 | AAC | Gly-60 | GGC |
| AQP6 N60G/G174N | Asn-60 | AAC | Gly-60 | GGC |
| | Gly-174 | GGG | Asn-174 | AAC |
| AQP0 G49N | Gly-49 | GGC | Asn-49 | AAC |
| AQP1 G57N | Gly-57 | GGG | Asn-57 | AAC |
| AQP2 G49N | Gly-49 | GGT | Asn-49 | AAT |

which disrupts hydrogen bonding in the single-file chain of water molecules (14). The amino acid sequence of AQP6 reveals that AQP6 potentially meets these mechanisms despite limited water permeability under basal conditions (15–17). AQP6 contains most of the conserved amino acid residues, including the NPA motifs. Also, the structure of AQP1 does not reveal mechanisms for gating, although most ion channels have well characterized gating mechanisms. Careful analysis of aquaporin sequence alignments with insight provided by structural models led us to identify a critical amino acid residue for anion permeability by AQP6.

## Materials and Methods

**Sequence Alignment and Structural Model.** Amino acid sequences of *Rattus norvegicus* (rat) AQP0 (P09011), AQP1 (NP_036910), AQP2 (NP_037041), AQP4 (NP_036957), AQP5 (NP_036911), and AQP6 (NP_071517) were aligned with CLUSTALX (Ver. 1.83). Regions containing transmembrane helix (TM) 2 and TM5 were selected based on x-ray crystallographic topology of AQP1 (12). The modeled structure of rat AQP6 was based on bovine AQP0, the most highly homologous sequence to AQP6 with a published atomic structure (18). The N-terminal 12- and C-terminal 28 amino acid residues of AQP6 were removed, because these two fragments do not have counterparts in AQP0 structure. Modeling was performed by the program JACKAL (http://trantor.bioc.columbia.edu/programs/jackal). Figures were prepared and rendered by SPDBV (3.7.5) or PYMOL (www.pymol.org).

**Plasmid Construction.** pXβG-ev1-AQP6 N60G, N60G/G174N, pXβG -ev1-AQP0 G49N, -AQP1 G57N, or -AQP2 G49N mutant was constructed with the QuikChange site-directed mutagenesis kit (Stratagene). Templates were pXβG-ev1-AQP6, -AQP0, -AQP1, or -AQP2. Table 1 lists the mutants used in this study. Mutations were confirmed by sequencing.

---

**Fig. 1.** Unique residues in AQP6 structure. (*A*) Sequence alignment of TM2 and TM5 of rat aquaporin proteins in the water-selective subgroup. Key residues implicated in AQP6 anion conductance including Asn-60, Thr-63, Trp-71, and Lys-72 are indicated in rectangles and numbered based on position in rat AQP6. (*B*) Structural model of AQP6, based on threading through the atomic structure of AQP0 (18). Two views, sagittal (*Left*) and cross-sectional (*Right*), highlighting the interaction between TM2 (in green) and TM5 (in orange), are shown in ribbon form. The side chain of Asn-60 is depicted with van der Waals space-filling spheres in CPK colors. The backbone atoms of Gly-174 are depicted with van der Waals space-filling spheres in magenta.

**Expression in Oocytes and Measurement of $P_f$.** Capped cRNAs were synthesized *in vitro* from *Xba*I-linearized pX$\beta$G -ev1 plasmids by using T3 RNA polymerase and purified with the RNeasy Mini kit from Qiagen (Valencia, CA). Defolliculated *X. laevis* oocytes were injected with 5 or 15 ng of cRNA or 50 nl of diethyl pyrocarbonate-treated water. Injected oocytes were incubated



**Fig. 2.** Electrophysiological analyses of AQP6 and N60G. (*A*) Representative currents of water-injected oocytes (*Top*), AQP6 oocytes (*Middle*), and N60G oocytes (*Bottom*) under NaCl solution (*Left*) and NaNO$_3$ solution (*Right*). The membrane potential was held at −50 mV and jumped to test potentials from +50 mV to −130 mV with 20 mV step voltage. The dashed line indicates the zero current level. (*B*) Representative I–V curves of water-injected oocyte (*Top*), AQP6 oocyte (*Middle*), and N60G oocyte (*Bottom*) in NaCl solution (open circles) or NaNO$_3$ solution (filled circles).

Liu *et al.*

**Fig. 3.** Rat AQP6 or mutants expressed in oocytes. *X. laevis* oocytes were injected with 15 ng of AQP6 WT, N60G, N60A, or N60S cRNA and cultured for 2.5 days. (*A*) Osmotic water permeability ($P_f$) of AQP6 or mutants. Arrhenius activation energy ($E_a$) of osmotic water permeabilities of N60G mutant oocytes and water-injected control oocytes (*Inset*). Osmotic-swelling assays were performed at 10, 20, or 30°C (mean $\pm$ SD, $n = 5$). (*B*) Confocal microscopy of oocytes injected with water, AQP6 WT, N60G, N60A, or N60S cRNA. The oocytes were stained by anti-rat AQP6 antibody. (*C*) Immunoblotting of membrane fraction from oocytes injected with water, rat AQP6 WT, N60G, N60A, or N60S cRNA.

for 2–3 days at 18°C in 200 milliosmolar modified Barth's solution. The oocyte swelling assay was used for osmotic water permeability measurement (19). Oocytes were transferred into modified Barth's solution diluted to 70 milliosmolar with distilled water, and the time course of volume increase was monitored at room temperature by videomicroscopy with an on-line computer (6, 16). The relative volume ($V/V_0$) was calculated from the area at the initial time ($A_0$) and after a time interval ($A_t$): $V/V_0 = (A_t/A_0)^{3/2}$. The coefficient of osmotic water permeability ($P_f$) was determined from the initial slope of the time course [$\mathrm{d}(V/V_0)/\mathrm{d}t$], initial oocyte volume ($V_0 = 9 \times 10^{-4}$ cm$^3$), initial oocyte surface area ($S = 0.045$ cm$^2$), and the molar volume of water ($V_w = 18$ cm$^3$/mol):

$$P_f = (V_0 \times \mathrm{d}(V/V_0)/\mathrm{d}t)/(S \times V_w \times (\mathrm{osm_{in}} - \mathrm{osm_{out}})).$$

**Electrophysiology.** Recordings were performed with isoosmotic NaCl solution (100 mM NaCl/2 mM KCl/1 mM MgCl$_2$/5 mM Hepes, pH 7.5) or isoosmotic NaNO$_3$ solution (100 mM NaNO$_3$/2 mM KCl/1 mM MgCl$_2$/5 mM Hepes, pH 7.5). The membrane potential of oocytes was controlled by using the two-microelectrode voltage-clamp technique. The command voltage was applied by a two-microelectrode voltage clamp amplifier (Axoclamp-2A, Axon Instruments, Foster City, CA) controlled by an IBM-compatible computer running PCLAMP software (Axon Instruments). Current signals were sampled at 100 $\mu$sec. In most experiments, the membrane potential was held at $V_{hold} = -50$ mV. To obtain a current–voltage relationship, the membrane potential was rapidly stepped from the holding potential to a series of values generated between $+50$ and $-130$ mV, each differing by 20 mV. The pulse duration was 100 msec, and currents from 10 runs were averaged to reduce noise. All measurements were performed at room temperature.

**Oocyte Immunofluorescence and Confocal Microscopy.** Oocytes were incubated in fixing solution (80 mM Pipes, pH 6.8/5 mM EGTA/1 mM MgCl$_2$/3.7% formaldehyde/0.2% Triton X-100) at room temperature for 4 h, transferred to methanol at $-20$°C for 24 h, equilibrated in PBS at room temperature for $\approx$2 h, incubated in PBS with 100 mM NaBH$_4$ at room temperature for 24 h, and bisected with blades. The oocytes were blocked by 2% BSA in PBS for 1 h at room temperature, incubated at 4°C

**Fig. 4.** The Gly to Asn mutants of AQP0, AQP1, AQP2, and AQP6 in oocytes. *X. laevis* oocytes were injected with 5 ng of AQP0, AQP1, AQP2, or the Gly to Asn mutants cRNA, or 15 ng of AQP6 N60G/G174N cRNA, and cultured for 2–3 days. (*A*) Osmotic water permeability ($P_f$) of AQP0 G49N, AQP1 G57N, AQP2 G49N, and AQP6 N60G/G174N. (*B*) Ion conductances of water injected, WT AQP6, or each mutant oocyte in NaCl solution (open columns) and NaNO$_3$ solution (closed columns). Conductances were calculated from slopes of I–V curves between +10 mV and −90 mV. Only the AQP6 oocyte showed conductance increase in NaNO$_3$ solution. (*C*) Confocal microscopy of oocytes injected with AQP0, AQP0 G49N, AQP1, AQP1 G57N, AQP2, AQP2 G49N, or AQP6 N60G/G174N cRNA. The oocytes were stained by the antibody against AQP0, AQP1, AQP2, or AQP6.

sequentially with rabbit anti-AQP6 antibody and Alexa Fluor 488 goat anti-rabbit IgG in blocking buffer (each for 24 h) and mounted in Fluoromount-G (Southern Biotechnology Associates). Pictures were taken with a PerkinElmer UltraView LCI confocal laser-scanning microscope.

**Oocyte Membrane Extraction and Immunoblotting.** Ten oocytes were homogenized together by pipetting up and down in hypotonic lysis buffer (7.5 mM sodium phosphate/1 mM EDTA, pH 7.5) including protease inhibitor mixture (Sigma). The oocyte yolk was removed by discarding the pellet after a 735 × *g* centrifugation at 4°C for 10 min. The supernatant was centrifuged again at 200,000 × *g*, 4°C, for 1 h; the membrane was harvested by collecting the pellet. The oocyte membrane was solubilized by 2% SDS, normalized by total protein amount with

BCA method (Pierce), and used in 12% SDS/PAGE. The proteins were transferred to a poly(vinylidene difluoride) membrane, probed with rabbit anti-rat AQP6 antibody and horseradish peroxidase-conjugated donkey anti-rabbit IgG (Amersham Pharmacia). The enhanced chemiluminescence detection system (Amersham Pharmacia) was used to visualize the specific immunoreactive proteins by exposure to autoradiographic films.

## Results

Sequence alignment of the mammalian aquaporins revealed that rat AQP6 has several unique amino acid residues: Tyr-34, Asn-60, Trp-71, and Lys-72 (Fig. 1*A*). These residues are conserved in mouse, rat, and human AQP6; all are located in TM1 and TM2 and loop B. Thr-63 and Lys-72 have been shown as key residues in AQP6 ion selectivity (8, 9). According to the atomic structural model of human AQP1, three large helical crossing angles stabilize crucial right-handed coiled-coil interactions; all have highly conserved glycine residues at the contact regions (10). For example, the fitting of ridges into grooves in TM2 and TM5 is mediated by two highly conserved glycine residues: Gly-57 and Gly-173 in human AQP1, respectively. Interestingly, we found that one of these glycine residues is replaced by an asparagine residue in rat AQP6 (Asn-60, Fig. 1*B*).

To test whether the unique asparagine residue (Asn-60) of rat AQP6 is critical for its unique anion permeability, Asn-60 was substituted by site-directed mutagenesis to Gly-60 (N60G mutant). In WT AQP6 oocytes, membrane currents exhibited substantial anion permeability. Slightly outward-rectifying currents were observed at pH 7.5 with a notable negative shift of the reversal potential immediately after replacement of the external buffer containing 100 mM NaCl with 100 mM NaNO$_3$ (Fig. 2 *A* and *B Middle*). N60G mutant oocytes and water-injected control oocytes failed to exhibit inducible currents by replacement of the external buffer containing 100 mM NaCl with 100 mM NaNO$_3$ at pH 7.5 (Fig. 2*A* and *B Bottom* and *Top*, respectively). We knew that lack of inducible currents in N60G mutant oocytes was not due to impaired membrane trafficking of the mutant protein, because the N60G mutant was localized at the plasma membrane as well as WT AQP6 (Fig. 3*B*). Neither N60A nor N60S mutant oocytes exhibited inducible currents in 100 mM NaNO$_3$ (pH 7.5) solution, although both were expressed at the oocyte plasma membranes (Fig. 3*B*).

We examined the osmotic water permeability of N60G mutant oocytes by swelling assay. Surprisingly, N60G mutant oocytes had significantly increased osmotic water permeability ($P_f = 131.62 \pm 16.11$ cm/s $\times 10^{-4}$) compared with water-injected or WT AQP6 oocytes ($P_f = 15.73 \pm 2.50$ cm per s $\times 10^{-4}$, $P_f = 12.40 \pm 5.22$ cm per s $\times 10^{-4}$, respectively) (Fig. 3*A*). The Arrhenius activation energy ($E_a$) was lower in N60G RNA-injected oocytes ($E_a < 5$ kcal/mol) than in water-injected control oocytes ($E_a > 10$ kcal/mol) (Fig. 3*A Inset*). Increase of osmotic water permeability in the N60G mutant was due neither to increased protein expression nor to changes in protein distribution (Fig. 3 *B* and *C*). These findings demonstrate that a single amino acid substitution at Asn-60 for Gly-60 not only abolishes anion permeability but also increases water permeability. The osmotic water permeability of N60G was not inhibited or activated by HgCl$_2$ (not shown). There was no evidence of protein glycosylation of the N60G mutant, although WT AQP6 has a 30-kD glycosylated form that is cleaved by both PNGase-F and Endo-H (Fig. 3*C* and ref. 15). These findings suggest that N60G may be different from WT AQP6 in terms of its *in vivo* 3D structure or configuration.

We next tested whether the N60G/G174N mutant, exchanging the asparagine residue from position 60 to position 174, recapitulates anion permeability. Neither anion permeability nor osmotic water permeability of N60G/G174N mutant oocytes was significantly increased over that of water-injected control
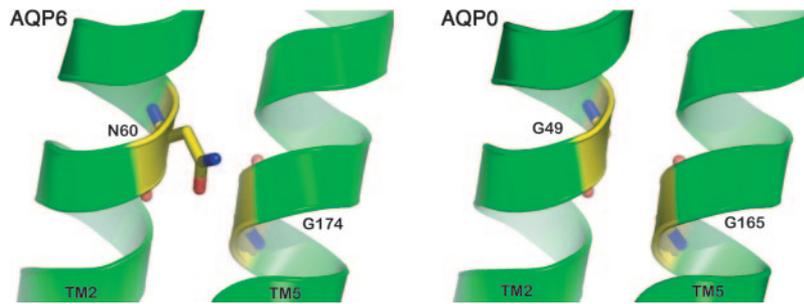
**Fig. 5.** Structural model highlighting the crossing point between TM2 and TM5. (*Left*) TM2 and TM5 of AQP6 structural model based on the AQP0 structure. Asn-60 and Gly-174 are highlighted. (*Right*) TM2 and TM5 in AQP0 crystal structure (18). The side chain of Asn-60 in AQP6 may affect the contact point between TM2 and TM5.

oocytes. This result may have been due to lack of expression of the N60G/G174N mutant at the plasma membrane of the oocytes (Fig. 4C).

To examine further the importance of the asparagine residue at the position in TM2 where it interacts with TM5, we introduced the reciprocal point mutation (Gly to Asn) in AQP0, AQP1, and AQP2. None of the reciprocal mutants revealed significant osmotic water permeability or ion permeability caused by impaired trafficking to the plasma membrane (Fig. 4).

## Discussion

Recent advances in structural biology have largely explained the biophysical properties of membrane channels in terms of selectivity, conductance, and gating (20, 21). The structural model of AQP1 and molecular dynamics simulations of water transport revealed how water molecules are rapidly transported through the pore, whereas protons are excluded (22, 23). The closest homologs of AQP6 are AQP0, AQP2, and AQP5; all belong to the classical group of aquaporins selectively permeated by water (17). AQP6, however, functions as an anion channel with limited water permeability, suggesting that subtle differences in the sequence of AQP6 may lead to major differences in biophysical function (8, 9). Here we have identified a critical amino acid residue for anion permeability of AQP6, Asn-60. We have demonstrated that a single amino acid substitution at Asn-60 for Gly-60 switches the function of AQP6 from that of an anion channel to that of a water-selective channel.

Asn-60 in AQP6 corresponds to Gly-57 in AQP1, which is conserved among all other mammalian aquaporins. The atomic model of AQP1 revealed that Gly-57 is located in the middle of TM2 and interacts with Gly-174, which is also conserved among all mammalian aquaporins in the middle of TM5. The fitting of ridges into grooves in TM2 and TM5 locks the two AQP1 helical bundles together near the 4-fold axis of the tetramer (11). This implies that the structure of AQP1 is relatively rigid, and that gating of AQP1 by conformational changes is unlikely. This rigid structure might be a general feature of aquaporins. It is extremely unusual for AQP6 to have an asparagine residue at the position corresponding to Gly-57 in human AQP1. Therefore, we

suspected that the residue in an important position from a structural point of view might be crucial to the unique anion permeability or gating of AQP6 (Fig. 5). We first used the human AQP1 structure because that of bovine AQP0 was not available during the study and manuscript preparation. Between human AQP1 and bovine AQP0, the glycine residues are conserved and the 3D structures at TM2 and TM5 are similar.

Our functional data support in another way the importance of glycine residues at the helical interaction sites for aquaporin structure formation. A N60G/G174N double AQP6 mutant and reciprocal glycine to asparagine mutations in AQP0, AQP1, and AQP2 all failed to traffic to the plasma membrane. These findings suggest that the interaction of TM2 and TM5 is precisely defined, and that subtle differences here lead to significant conformational changes. It may be necessary but not sufficient to have an asparagine residue at its key position for anion permeability.

We have demonstrated that Thr-63 and Lys-72 are critical residues in AQP6 ion selectivity (8, 9). Other residues, including Thr-63 and Lys-72, may allow AQP6 to have an asparagine residue at its position corresponding to the well conserved Gly-57 in hAQP1 without impairing protein folding. Also, we suspect that the pore diameter of AQP6 at its narrowest point is significantly wider than that of AQP1, because AQP6 is permeated by $SCN^-$ and $NO_3^-$. The pore in AQP1 narrows to 2.8 Å, which is too narrow for these anions (24). On the other hand, the N60G mutant may have a similar pore diameter, because it is permeated by water but not by anions.

Having identified notable functional differences between WT AQP6 and the N60G mutant, we feel it is crucial to solve the structures of both WT AQP6 and the N60G mutant. We expect that a structural comparison of these mutants will give us a better understanding of how AQP6 is permeated by anions and why other aquaporins are not permeated by any ions.

1. Agre, P., King, L. S., Yasui, M., Guggino, W. B., Ottersen, O. P., Fujiyoshi, Y., Engel, A. & Nielsen, S. (2002) *J. Physiol.* **542,** 3–16.
2. Stroud, R. M., Savage, D., Miercke, L. J. W., Lee, J. K., Khademi, S. & Harries, W. (2003) *FEBS Lett.* **555,** 79–84.
3. Tsunoda, S.P., Wiesner, B., Lorenz, D., Rosenthal, W. & Pohl, P. (2004) *J. Biol. Chem.* **279,** 11364–11367.
4. Ilan, B., Tajkhorshid, E., Schulten, K. & Voth, G. A. (2004) *Proteins* **55,** 223–228.
5. Burykin, A. & Warshel, A. (2004) *FEBS Lett.* **570,** 41–46.
6. Chakrabarti, N., Roux, B. & Pomes, R. (2004) *J. Mol. Biol.* **343,** 493–510.
7. Yool, A. J., Stamer, W. D. & Regan, J. W. (1996) *Science* **273,** 1216–1218.
8. Yasui, M., Hazama, A., Kwon, T. H., Nielsen, S., Guggino, W. B. & Agre, P. (1999) *Nature* **402,** 184–187.
9. Ikeda, M., Bitz, E., Kozono, D., Guggino, W. B., Agre, P. & Yasui, M. (2002) *J. Biol. Chem.* **277,** 39873–39879.
10. Hazama, A., Kozono, D., Guggino, W. B., Agre, P. & Yasui, M. (2002) *J. Biol. Chem.* **277,** 29224–29230.
11. Murata, K., Mitsuoka, K., Hirai, T., Walz, T., Agre, P., Heymann, J. B., Engel, A. & Fujiyoshi, Y. (2000) *Nature* **407,** 599–605.
12. Sui, H., Han, B. G., Lee, J. K., Walian, P. & Jap, B. K. (2001) *Nature* **414,** 872–878.
13. Schneider, D., Liu, Y., Gerstein, M. & Engelman, D. M. (2002) *FEBS Lett.* **532,** 231–236.

14. Kozono, D., Yasui, M., King, L. S. & Agre, P. (2002) *J. Clin. Invest.* **109,** 1395–1399.
15. Yasui, M., Kwon, T. H., Knepper, M. A., Nielsen, S. & Agre, P. (1999) *Proc. Natl. Acad. Sci. USA* **96,** 5808–5813.
16. Ma, T., Frigeri, A., Skach, W. & Verkman, A. S. (1993) *Biochem. Biophys. Res. Commun.* **197,** 654–659.
17. Ma, T., Yang, B., Umenishi, F. & Verkman, A. S. (1997) *Genomics* **43,** 387–389.
18. Harris, W. E., Akhavan, D., Miercke, L. J. & Stroud, R. M. (2004) *Proc. Natl. Acad. Sci. USA* **101,** 14045–14050.
19. Preston, G. M., Carroll, T. P., Guggino, W. B. & Agre, P. (1992) *Science* **256,** 385–387.
20. MacKinnon, R. (2004) *Angew. Chem. Int. Ed.* **43,** 4265–4277.
21. Agre, P. (2004) *Angew. Chem. Int. Ed.* **43,** 4278–4290.
22. de Groot, B. L. & Grubmuller, H. (2001) *Science* **294,** 2353–2357.
23. Tajkhorshid, E., Nollert, P., Jense, M. O., Miercke, L. J., O'Connell, H., Stroud, R. M. & Schulten, K. (2002) *Science* **296,** 525–530.
24. Smith, S. S., Steinle, E. D., Meyerhoff, M. E. & Dawson, D. C. (1999) *J. Gen. Physiol.* **114,** 799–817.